Deficiency of B vitamins leads to cholesterol-independent atherogenic transformation of the aorta

Gunter Almer
Clinical Institute for Medical and Chemical Laboratory Diagnostics, Medical University of Graz
Peter Opriessnig
Department of Neurology, Division of General Neurology, Medical University of Graz, Department of Neurology, Department of Radiology, Division of Pediatric Radiology, Medical University of Graz
Heimo Wolinski
Institute of Molecular Biosciences, University of Graz
Gerhard Sommer
Institute of Biomechanics, Graz University of Technology
Clemens Diwoky
Institute of Molecular Biosciences, University of Graz
Margarete Lechleitner
Gottfried Schatz Research Center, Molecular Biology and Biochemistry, Medical University of Graz
Dagmar Kolb
Gottfried Schatz Research Center, Cell Biology, Histology and Embryology, Medical University of Graz, Center for Medical Research, Ultrastructure Analysis, Medical University of Graz
Vladimir Bubalo
Division of Biomedical Research, Medical University of Graz
Markus Brunner
Institute of Molecular Biosciences, University of Graz,
Andreas Schwarz
Institute of Molecular Biosciences, University of Graz,
Gerd Leitinger
Gottfried Schatz Research Center, Cell Biology, Histology and Embryology, Medical University of Graz
Garbriele Schoiswohl
Institute of Molecular Biosciences, University of Graz, Department of Pharmacology and Toxicology, University of Graz
Gunther Marsche
Medical university of Graz
Tobias Niedrist
Medical University of Graz

Silvia Schauer
Diagnostic and Research Institute of Pathology, Medical University of Graz
Wolfgang Oswald
Department of Surgery, Clinical Division of Vascular Surgery, Medical University of Graz
Andrea Groselj-Strele
Center for Medical Research, Computational Bioanalytics, Medical University of Graz
Marget Paar
Otto Loewi Research Center, Physiological Chemistry, Medical University of Graz
Gerhard Cvirn
Otto Loewi Research Center, Physiological Chemistry, Medical University of Graz
Gerald Hoefler
Diagnostic and Research Institute of Pathology, Medical University of Graz
Gerald Rechberger
Department of Molecular Biosciences, University of Graz https://orcid.org/0000-0002-0071-317X
Markus Herrmann
Clinical Institute for Medical and Chemical Laboratory Diagnostics, Medical University of Graz
Sasa Frank
Gottfried Schatz Research Center, Molecular Biology and Biochemistry, Medical University of Graz
Gerhard Holzapfel
Institute of Molecular Biosciences, University of Graz, Department of Structural Engineering, Norwegian University of Science and Technology
Dagmar Kratky
Medical University of Graz https://orcid.org/0000-0003-1357-7573
Harald Mangge
Clinical Institute for Medical and Chemical Laboratory Diagnostics, Medical University of Graz
Gerd Hörl
Otto Loewi Research Center, Physiological Chemistry, Medical University of Graz
Oksana Tehlivets (**oksana.tehlivets@uni-graz.at**)
University of Graz https://orcid.org/0000-0003-1650-5014

Research Article

Keywords: preclinical models, rabbits, balloon catheter injury, atherosclerosis, B vitamin deficiency, homocysteine

Posted Date: March 17th, 2022

DOI: https://doi.org/10.21203/rs.3.rs-1358736/v2

Abstract

Atherosclerosis is the leading cause of cardiovascular disease, which is responsible for the majority of deaths worldwide. Elevated plasma homocysteine is an independent risk factor for atherosclerosis and is strongly linked to cardiovascular mortality. However, lack of reproducible and controlled induction of atherosclerotic lesions in preclinical animal models limits atherosclerosis research. Here, we developed the first automated system for vessel wall injury that leads to more homogenous damage and more pronounced atherosclerotic plaque development at low balloon pressure in a rabbit model of atherosclerosis, and used this system to investigate the risk factor interplay. Already in the absence of hypercholesterolemia, deficiency in vitamins and choline required for homocysteine metabolization results in atherogenic transformation of the aorta i.e. impairment of its biomechanical properties, alteration of collagen organization as well as macrophage and lipid accumulation, and aggravation of atherosclerosis including significantly altered water diffusion and impaired vascular reactivity in its presence.

Summary

Only fifty percent of atherosclerosis incidence can be explained by established risk factors. Using technically refined injury methodology and modular dietary design to study atherogenesis in rabbits this work unveils deficiency of B vitamins as cholesterol-independent and interacting risk factor.

Introduction

Cardiovascular disease, the leading cause of death worldwide, is mostly due to the development of atherosclerosis (Lefkowitz and Willerson, 2001). However, only 50% of the incidence of atherosclerosis today can be explained by known risk factors such as hypercholesterolemia (Lefkowitz and Willerson, 2001). Rabbits and mice are the most common animal models used to study atherosclerosis (Veseli et al., 2017). Whereas mice develop atherosclerosis only after genetic manipulation, e.g. apolipoprotein E (ApoE) or low-density lipoprotein receptor (Ldlr) knockout mice (Getz and Reardon, 2006), rabbits on a high-fat diet spontaneously develop foam cell-rich plaques (fatty streaks) resembling human atheroma (Phinikaridou et al., 2009). Injury to the arterial wall shortens the time required for advanced lesions to form in response to hyperlipidaemia (Phinikaridou et al., 2009). In most cases, vascular injury in atherosclerotic animal models is achieved by repeated retraction of an inflated balloon tip catheter within an artery (Asada et al., 1996). Here, we developed an automated system for balloon-mediated injury (JURY) and compared this technique with the classical manual injury of the aorta in the rabbit atherosclerosis model. JURY controls both the balloon pressure and catheter retraction speed and can therefore standardize and optimize vessel wall injury.

Hyperhomocysteinemia (HHcy), characterized by elevated plasma homocysteine (Hcy) levels, is an independent risk factor for atherosclerosis, increases the risk in combination with hypercholesterolemia and is closely associated with cardiovascular mortality (Refsum et al., 1998, Vollset et al., 2001). In accordance, dietary induction of HHcy by folate, vitamin B_6 and B_{12} deprivation, high methionine levels, or genetic blockade of Hcy metabolization exacerbates atherosclerosis in mouse models (Hofmann et al., 2001, Wang et al., 2003). Choline is also required for Hcy metabolization and its deficiency is linked to HHcy (Teng et al., 2012). HHcy is present in 5-10% of the general population, in up to 30% of the elderly and in 70% of men over 80 years of age (Refsum et al., 1998, Selhub et al., 1993, Xu et al., 2020). Two-thirds of HHcy incidence is due to deficiency of vitamins required for Hcy metabolization (Selhub, 2006). Here we show that a diet deficient in folate (20%), vitamin B_6 (20%) and B_{12} (0%) as well as choline (10%) (VCDD) required for Hcy metabolization leads to atherosclerosis aggravation in the presence of hypercholesterolemia and atherogenic transformation of the aorta in its absence in the balloon-injured rabbit model of atherosclerosis. In summary, this study demonstrates i) an innovative technique for vessel wall injury, ii) a new atherosclerotic rabbit model that can be used to study lipid- and Hcy-related risk factors simultaneously, and iii) a combination of both to study atherosclerosis.

Results

Development of JURY-controlled balloon injury technique to improve usability of animal models of atherosclerosis

The widely used techniques to induce atherogenesis do not ensure controlled, reproducible denudation of the endothelium of the aorta and/or arteries. We have developed and tested an automated device, which allows reproducible injury by controlling pressure and retraction speed, and regulation of injury severity. The JURY system displays, records and controls the pressure of the inflated balloon in real-time and retracts the balloon at a predefined speed. In brief, a saline filled 4F40 Fogarty catheter was inserted in the femoral artery and advanced into the aorta abdominalis. After reaching the predefined start position the balloon was inflated and retracted with pre-adjusted speed over a distance of 9 cm. A detailed description of the device, surgery and the JURY-controlled injury is given in supplement 1 and 2. To optimize and diversify the injury procedure, two different target pressures, 1.2 and 1.8 bar, as well as single or repeated retractions of the catheter at constant speed were applied.

-

Initially, we compared three different injury protocols: 1) classical “blind” injury, during which pressure and retraction speed were manually regulated without pressure monitoring, 2) modification of the classical “blind” injury by manual adjustment of the pressure based on displayed pressure data, and 3) fully automated pressure- and retraction-controlled injury system (JURY device) with pressure data and

motor steps for balloon inflation/deflation being displayed, recorded and adjusted automatically. The JURY-controlled injury exhibited the lowest variation of the target pressure (Fig. 1A). The classical injury without pressure monitoring ("blind") showed the highest and with pressure monitoring medium pressure fluctuations. The JURY device compensates for anatomy-related variations of the vessel diameter by decreasing the balloon volume during retraction as observed at sites of narrowing of the aorta abdominalis (Fig. 1A3). Thus, vessel wall injury with the JURY device can be performed on vessels of different thickness (e.g. aortas from animals of different size and age) with identical mechanical stress. Moreover, we observed large variations in retraction speed with the manual techniques. A constant retraction speed was only achieved by the JURY system.

Comparison of the automated JURY-controlled and the manual pressure-adjusted injury (with pressure monitoring, manual pressure adjustment and manual retraction) revealed that use of the JURY device enables complete endothelial denudation already at 1.2 bar with single retraction, whereas the manual pressure-adjusted injury with the same settings resulted only in partial denudation of the endothelium (Fig. 1B3). Both injury types significantly reduced acetylcholine-induced relaxation of the aortic rings compared to untreated controls (Fig. 1B1, 2 way ANOVA, JURY, 95% CI [-49.93, -35.85], $p<0.001$; manual, 95% CI [-35.21, -17.54], $p<0.001$; injury type $F(2,48)=66.44$, $p<0.001$). Importantly, the automated JURY-controlled injury also significantly reduced acetylcholine-induced relaxation compared to the manual-pressure-adjusted injury (Fig. 1B1, JURY-manual, 95% CI [-22.02, -11.01], $p<0.001$), possibly due to incomplete denudation, indicating that automated injury at low pressure and single retraction was more efficient than manual injury. Neither injury protocol altered sodium nitroprusside-induced relaxation compared to untreated controls (Fig. 1B2, JURY, 95% CI [-4.865, 16.12], $p=0.593$; manual, 95% CI [-2.596, 18.16], $p=0.216$) indicating that the damage was confined to the endothelium and did not affect the underlying smooth muscle cells. The statistical analysis is shown in S7. Immunohistological staining confirmed that JURY-controlled balloon injury resulted in complete denudation of the endothelial layer (Fig. 1B3c), whereas the manual pressure-adjusted injury with the same settings resulted only in partial denudation of the endothelium (Fig. 1B3b).

Analysis of atherosclerotic plaque development in rabbits fed high cholesterol Western-type diet (HCD) for 6 weeks post-injury revealed that the automated JURY-controlled injury at 1.2 bar and single retraction resulted in the development of significantly thicker and more homogenous atherosclerotic plaques compared to the manual pressure-adjusted injury with the same settings (Fig. 2A1 and B; condition 3 vs 2; $U=32$, $p=0.026$, $p_{adj}=0.052$). Increasing the balloon pressure to 1.8 bar and the number of retractions to three (severe injury protocol) significantly increased thickness of the aortic wall in both JURY and manual pressure-adjusted injury (Fig. 2A1 and B; condition 5 vs 3; $U=22$, $p=0.038$, $p_{adj}=0.076$; condition 4 vs 2; $U=24$, $p=0.010$, $p_{adj}=0.020$, respectively) compared to minimal injury protocol (1.2 bar and single retraction). Under severe injury conditions, no differences in plaque size were observed between

automated and manual injury in NZW rabbits (Fig. 2A1 and B; condition 5 vs 4, U=8, p=1.000, p_{adj}=2.000). JURY-controlled endothelial denudation led to comparable atherosclerotic plaque formation also in Hyla/Wildtype crossbreds (cbHyla) (Fig. 2A1 and B). The severe injury protocol significantly increased thickness of the aortic wall compared to minimal injury protocol when the JURY device was used in cbHyla rabbits (Fig. 2A1; condition 8 vs 6; U=24, p=0.016, p_{adj}=0.038). Notably, in cbHyla animals, JURY-controlled injury at 1.8 bar with three pull-backs resulted in more homogenous atherosclerotic plaque formation with non-significantly increased plaque thickness compared to the manual pressure-adjusted injury (Fig. 2A1 and B; condition 8 vs 7, U=20, p=0.151, p_{adj}=0.302).

Diffusion tensor MRI allows assessment of microscopic fiber orientation and cellular structure by measuring FA of water diffusion (Coolen et al., 2018). A higher FA corresponds to healthy intima/media tissue, whereas low FA is associated with ageing and an alteration of arterial tissue microstructure (Opriessnig et al., 2016, Tornifoglio et al., 2020). While in NZW rabbits the JURY-controlled minimal or severe injury protocols resulted in non-significantly decreased FA compared to the manual procedures with the same settings (Fig. 2A2; condition 3 vs 2, U=6, p=0.065, p_{adj}=0.130 and 5 vs 4; U=3, p=0.200, p_{adj}=0.400, respectively) in cbHyla rabbits both the severe JURY-controlled protocol compared to the minimal JURY-controlled protocol or compared to severe manual protocol led to significantly decreased FA (Fig. 2A2; condition 8 vs 6 and condition 8 vs 7; both U=0, p=0.008, p_{adj}=0.016).

Deficiency of B vitamins leads to atherogenic transformation of the aorta in the absence of hypercholesterolemia and aggravated atherosclerosis in its presence

Feeding JURY-injured rabbits a diet deficient in folate, vitamins B_6, B_{12} and choline required for Hcy metabolization (VCDD) in the absence or presence of hypercholesterolemia resulted in non-significant thickening of the aortic wall compared to chow diet or HCD, respectively (Fig. 3A, Kruskal-Wallis-Test, H=21.742, SD-VCDD, p=0.157, p_{adj}=0.944 and HCD-VCD/HCD, p=0.143, p_{adj}=0.855). However, more pronounced and highly significant aortic wall thickening in response to VCD/HCD in comparison to chow diet (p=0.000, p_{adj}=0.000) than in response to HCD alone (p=0.011, p_{adj}=0.068), suggests that VCDD indeed plays an important role in aortic thickening in the presence of HCD (Fig. 3A). Furthermore, VCD/HCD but not HCD alone leads to significantly decreased FA compared to chow diet (Fig. 3B, H=9.063, p=0.006, p_{adj}=0.035 and p=0.563, p_{adj}=1.000, respectively), further suggesting that VCDD is synergistic with HCD in atherogenic transformation of the aorta. Detection of lipid droplets and macrophages in the aortic neointima in response to VCDD alone, their increased abundance in response to VCD/HCD (Fig. 3C and D) as well as increased low-density lipoprotein (LDL)-cholesterol in response to

combined diet (Fig. 3E) indicate that VCDD induces atherogenic alterations in the aorta already in the absence of hypercholesterolemia and increases atherogenicity of HCD. Very low-density lipoprotein (VLDL)-triglyceride and free glycerol were also elevated in response to VCD/HCD compared to HCD alone, indicating a synergistic effect of the combined diet not only on cholesterol but also triglyceride metabolism (Fig. 3F). Notably, VCDD resulted only in a slight, non-significant accumulation of circulating Hcy, had no effect on total plasma cholesterol or triglyceride concentrations, food intake or weight gain, and did not result in any pathological changes of the liver compared to rabbits fed chow diet (supplement 3-5).

Second harmonic generation (SHG) and coherent anti-Stokes Raman scattering (CARS) microscopy revealed collagen disorganization, and confirmed lipid accumulation and accumulation of cellular structures reminiscent of macrophages in the aortic wall of JURY-injured rabbits fed VCDD (Fig. 4A and B). VCD/HCD resulted in further collagen disorganization as well as increased numbers of macrophages/foam cells in the plaque area compared to any other diet (Fig. 4A and B). Electron microscopic analysis of the aortic media further supported an independent impact of VCDD. Already in the absence of HCD, VCDD resulted in an accumulation of lipid droplets and dilated endoplasmic reticulum (ER) in smooth muscle cells and fibroblasts in the aorta of JURY-injured rabbits, which was not observed in the rabbits fed chow diet (Fig. 5A and B). Dilated ER was only observed in rabbits fed VCDD, both in the absence and presence of HCD (Fig. 5B and D). Finally, in addition to lipid droplet and macrophage accumulation, VCD/HCD also led to widened spacing between elastic fibers and smooth muscle cells in the aortic media, which was not observed in chow diet-fed rabbits, thereby confirming the detrimental effects of VCD/HCD (Fig. 5D).

Biaxial extension tests revealed that VCDD induces mechanical stiffening of the aorta even in the absence of hypercholesterolemia (Fig. 6A and B, Kruskal-Wallis-Test, SD-VCDD, $H=13.780$, $p=0.007$, $p_{adj}=0.042$ at 1.3 stretch circumferential direction and $H=8.980$, $p=0.035$, $p_{adj}=0.208$ at 1.4 stretch longitudinal direction, respectively and supplement 6). Under our study conditions, HCD did not lead to aortic stiffening (Fig. 6A and B, SD-HCD, $p=0.807$, $p_{adj}=1.000$ at 1.3 stretch circumferential direction and $p=0.944$, $p_{adj}=1.000$ at 1.4 stretch longitudinal direction; VCDD-VCD/HCD, $p=0.940$, $p_{adj}=1.000$ at 1.3 stretch circumferential direction and $p=0.806$, $p_{adj}=1.000$ at 1.4 stretch longitudinal direction and supplement 6). In contrast, VCDD resulted in significantly increased aortic stiffening in circumferential direction, when combined with HCD compared to HCD alone (Fig. 6A and B, HCD-VCD/HCD, $p=0.011$, $p_{adj}=0.066$ at 1.3 stretch circumferential direction and supplement 6), suggesting that VCDD has a stronger impact on aortic elasticity than HCD. Furthermore, feeding rabbits VCD/HCD resulted in massive impairment of K^+-induced contraction of the aortic rings compared to any single diet, indicating that the combination of VCDD and HCD is particularly harmful to the aorta (Fig. 6C, 1 way ANOVA, $p<0.001$, $p_{adj}<0.001$). While neither HCD or VCD/HCD led to significant impairment of norepinephrine-reactivity of

aortic rings compared to control diet (Fig. 6D, 2 way ANOVA, HCD-SD, p>0.999, VCD/HCD-SD, p=0.214; diet F(3,76)=13.46, p<0.001), both HCD and VCD/HCD resulted in significantly impaired norepinephrine-reactivity compared to VCDD (Fig. 6D, HCD-VCDD, p=0.017, VCD/HCD-VCDD, p=0.002) suggesting a role of VCDD in norepinephrine-induced contraction. Furthermore, while HCD had no effect on acetylcholine-relaxation of aortic rings compared to control diet (Fig. 6E, HCD-SD, p=0.106; diet F(3,76)=3.465, p=0.020), VCDD and VCD/HCD resulted in significant impairment of acetylcholine-relaxation (VCDD-SD, p=0.004, VCD/HCD-SD, p<0.001) suggesting a role of VCDD in acetylcholine-relaxation. Neither HCD, VCDD or VCD/HCD had a significant effect on sodium nitroprusside-relaxation of aortic rings compared to SD (Fig. 6F, SD-HCD, SD-VCDD, SD-VCD/HCD, p>0.999; diet F(3,74)=3.172, p=0.029), further indicating that the damage was confined to the endothelium and did not affect the underlying smooth muscle cells. Widened spacing between elastic fibers and smooth muscle cells in the media in response to VCD/HCD (Fig. 5D) suggest a direct link to impaired vascular reactivity. Altogether, our data indicate that VCDD already in the absence of HCD induces atherogenic transformation of the aorta as well as aggravates atherosclerosis in its presence.

Discussion

Although atherosclerotic cardiovascular disease was previously considered to be a problem of industrialized countries, now it is common worldwide (Libby, 2021). Preclinical animal models play a central role in atherosclerosis research (Veseli et al., 2017), but it is unclear how closely they mimic human atheroma. Atherosclerosis develops over very long periods of time and today only half of its incidence can be explained by established risk factors, with many young or middle-aged individuals displaying asymptomatic and subclinical atherosclerotic lesions (Lefkowitz and Willerson, 2001, Libby, 2021). Despite the identification of a number of risk factors that drive arterial wall alterations, such as dyslipidemia, endothelial dysfunction, inflammation, immune disease, malnutrition and lifestyle (Libby, 2021), a clear hierarchy is not evident. A deeper understanding of the risk factors for atherosclerosis and revised concepts of atherogenesis are urgently needed to improve treatment of cardiovascular disease and to understand its interplay with associated diseases such as COVID-19 (Nishiga et al., 2020). Due to similarities to human lipoprotein metabolism the rabbit is a good model to study the interaction of various atherosclerotic risk factors (Phinikaridou et al., 2009). HCD is a potent trigger of atherogenesis in preclinical animal models, however, feeding HCD over prolonged time is toxic. Injury of the arterial wall accelerates formation of advanced lesions in response to hyperlipidemia, helping to overcome the toxic effects (Phinikaridou et al., 2009). Nonetheless, the commonly used classical injury techniques lead to non-reproducible/uneven atherosclerotic plaque development, thereby limiting the high potential of such models.

To standardize atherosclerotic rabbit models, we have developed an automated injury technique (JURY) that increases the reproducibility and homogeneity of atherosclerotic lesion formation. The JURY device compensates for anatomical differences in vessel diameter and keeps friction effects more constant due

to automated retraction system. JURY is connected to a computer enabling adjustment of injury parameters, recording and display of balloon pressure data on a monitor in real-time. This technique allows induction of mild injury already at 1.2 bar and single retraction, limiting the injury to the endothelial layer and reducing undesirable effects such as aortic aneurysms, which can be caused by high pressure and/or repeated denudation steps. Importantly, the automation of the vessel wall injury leads to complete denudation of the endothelium and more homogeneous and reproducible atherosclerotic plaque formation compared to manual injury. Balloon pressure is indeed a critical parameter influencing not only the severity of vascular injury but also subsequent intimal hyperplasia and vasomotor responses (Asada et al., 1996). The damage produced by our method corresponds to type II injury (Ip et al., 1990) and could be induced over the entire intended area, allowing a more comprehensive analysis and extended applicability of the model. The comparison of the automated JURY-controlled injury with the classical “blind” and manual pressure-adjusted denudation demonstrates that the automated injury outperforms the other techniques.

MRI analyses applied in this study were sensitive to detect significant differences between the various injury scenarios. Diffusion tensor imaging is frequently used to evaluate tissue integrity and is able to detect slight alterations earlier than conventional MRI imaging (Tamura et al., 2021). FA was already shown to be highly sensitive to changes in microstructural composition of the arterial tissue (Tornifoglio et al., 2020). Indeed, our data further suggest that FA is a sensitive indicator of arterial wall remodeling offering new insights into reorganization of connective tissue during atherogenesis.

In the present study, the capabilities of the JURY device were far from exhausted, and more sophisticated injury scenarios could be developed based on the results obtained. Indeed, repeated denudation and/or more severe injury parameters result in formation of complicated plaques and thrombi (Yamashita et al., 2004), however, under the described injury conditions thrombi were not observed in this study. The JURY device is superior in pressure maintenance and is, to our knowledge, the first motorized catheter retraction system. Furthermore, we consider that standardization of the injury method allows reduction of the number of experimental animals needed.

The incidence of atherosclerosis cannot sufficiently be explained by established risk factors (Lefkowitz and Willerson, 2001). Establishing and understanding of further risk factors for atherosclerosis is, therefore, of utmost importance. Mouse models widely used in preclinical atherosclerosis research, however, do not assess the potential proatherogenic effects of elevated Hcy under conditions of unblocked but compromised lipoprotein remnant clearance characteristic for humans (Hofmann et al., 2001, Wang et al., 2003). Not only Hcy itself, but also vitamins required for Hcy metabolism and associated with the occurrence of HHcy are still debated regarding their possible role in subclinical AS

and/or its progression (Selhub, 2006, Vermeulen et al., 2000). Rabbits with similar to humans lipoprotein metabolism can, therefore, serve as a good model, not only to study hyperlipidemia-induced atherosclerosis or to be used in preclinical drug screening, but also to dissect the role of Hcy, its associated metabolites (Visram et al., 2018, Perla-Kajan et al., 2016) as well as vitamins and choline or other risk factors in atherosclerosis development. Increased reproducibility of vessel injury as well as increased length of evenly injured vessel area due to use of automated injury will reduce the number of animals required in such studies.

We used a diet reduced in folate, vitamins B_6, B_{12} and choline to block Hcy metabolization and to investigate the effects of this diet on the development of atherosclerosis in the absence and presence of hypercholesterolemia in rabbits. While our data do not allow to conclude whether depletion of vitamins B_{12}, or reduced availability of folate, vitamin B_6 or choline, or an accumulation of Hcy is responsible for the changes observed, they show that combination of HCD and VCDD markedly increased atherogenic transformation of the aorta, suggesting that hypercholesterolemia and interference with Hcy metabolism or other consequences of folate vitamin B_6, B_{12} and choline reduction have synergistic effects on atherosclerosis development. In accordance, it has been previously reported that low serum vitamin B_{12} levels are associated with unfavorable lipid profiles in humans (Al-Musharaf et al., 2020). The massively impaired vascular reactivity in response to VCD/HCD further confirms that the combined diet is particularly harmful to the aorta. Moreover, our data link VCDD to enhancement of norepinephrine-induced contraction probably due to altered biomechanical properties of the aorta as well as impairment of acetylcholine-relaxation. Supporting this notion, Hcy was shown to be associated with endothelial dysfunction (Liang et al., 2021), and the combination of HCD and methionine, a precursor of Hcy, results in virtually abolished endothelium-dependent relaxation (Zulli et al., 2003).

Furthermore, VCDD leads to atherogenic transformation of the aorta already in the absence of HCD. Feeding VCDD to balloon-injured rabbits results in aortic stiffening and accumulation of lipids and macrophages in the neointima, suggesting that VCDD can induce atherogenic transformation of the aorta independently of hypercholesterolemia. Aortic wall elasticity drops in atherosclerosis (Cecelja and Chowienczyk, 2012) and pulse wave velocity, which is increased in stiffer arteries, is an independent predictor of cardiovascular morbidity and mortality (Cecelja and Chowienczyk, 2012). Compromised organization of collagen (Perla-Kajan et al., 2016) or elastin (Hubmacher et al., 2010), or vessel calcification (Karger et al., 2020), which are all linked to elevated Hcy, may induce aortic stiffening in response to VCDD. Noteworthy, elastin fragmentation in atherosclerosis mice leads to a highly unstable plaque phenotype (Van der Donckt et al., 2015) and reduced aortic burden (Chen et al., 2019).

Accumulation of lipids, macrophages and dilated ER, as well as aortic stiffening in the absence of hypercholesterolemia imply that VCDD induces both different and similar atherogenic pathways in the aortic wall compared to HCD. The lack of significant increase in plasma Hcy in response to VCDD may be due to its metabolization to S-adenosyl-L-homocysteine (AdoHcy) and Hcy-thiolactone (Perla-Kajan et al., 2016), which were not determined. Our data also show that even these mild conditions, either via disruption of the Hcy metabolism and/or due to independent consequences of vitamin and choline deficiency, cause atherogenic transformation of the aorta already in the absence of hypercholesterolemia and drastically aggravate atherosclerosis in its presence. Indeed, Hcy/AdoHcy has already been linked to LDL-cholesterol in humans (Dong et al., 2016) as well as cholesterol metabolism (Mikael et al., 2006), lipolysis (Yan et al., 2020), VLDL secretion (Werstuck et al., 2001), and decreased mRNA and protein levels of PPARa/g (Yideng et al., 2008). Hcy is also linked to the upregulation of cholesterol/triglyceride biosynthesis and uptake in vascular endothelial and aortic smooth muscle cells mediated by sterol regulatory element-binding proteins (Werstuck et al., 2001). Since VCDD does not increase plasma triglyceride and total cholesterol, lipid accumulation in the aortic wall of rabbits fed VCDD suggests deregulation of intracellular lipid metabolism, which is further supported by increases in LDL-cholesterol and VLDL-triglyceride in response to VCD/HCD compared to HCD. Detection of macrophages in the absence of hypercholesterolemia indicates activation of inflammation by VCDD. Furthermore, elevated Hcy may activate matrix metalloproteinases (MMPs) by increasing reactive oxygen species and trigger smooth muscle cell migration within the vessel via MMP-dependent collagen degradation (Vacek et al., 2015).

In summary, significant thickening of the aortic wall, massive impairment of vascular reactivity, altered FA and increased accumulation of lipids and macrophages in the neointima indicate a stronger impact of the HCD on atherogenic transformation of the aorta when combined with VCDD. VCDD has also an independent impact on atherogenic transformation of the aortic wall by inducing accumulation of lipids and macrophages, dilatation of ER as well as loss of vessel elasticity. Thus, the rabbit model of experimental atherosclerosis described here clearly shows that there are other factors that can exacerbate atherosclerosis triggered by high cholesterol as well as induce independent atherosclerotic changes in the aortic wall. The JURY technique in combination with this model offers new tools to advance atherosclerosis research and expand the horizon for new therapeutic strategies.

Materials And Methods

2.1. JURY device for pressure- and retraction-controlled balloon denudation in rabbits

The JURY device for pressure- and retraction-controlled vessel wall injury was developed for the use of balloon tip catheters in rabbits. Various Fogarty embolectomy catheters (3F40, 3F80, 4F40 and 4F80; mpö pfm GesmbH, Austria) were tested and selected according to the average size of the adult rabbit aorta abdominalis. *In vitro* tests showed that the Fogarty 4F40 catheter exhibits the best compliance for

mechanical pressure control in the experimental setting and that a threshold pressure of 1.2 bar is required to expand the balloon of the 4F40 catheter.

2.2. Animal experiments

All animal experiments were approved by the Austrian Federal Ministry of Education, Science and Research (BMWF-66.010/01 1 I-II/3b/2012 and 66.010_0070-V_3b_2018). For the study, 4- to 6-month old male rabbits (New Zealand White rabbits (NZW rabbits), Charles River (France), Schitkowitz (Austria) and Hyla/Wildtype crossbreds (cbHyla, Schitkowitz Austria)) were used. Prior to the studies, the rabbits were acclimatized for 2-4 weeks. Rabbits were set on special diets after or before surgery. The diets used included an unpurified complete chow diet (standard diet, SD) for full nutritional conditions and purified special diets either enriched with 1% cholesterol (HCD), deficient in vitamins and choline required for Hcy metabolization (no vitamin B_{12}, 20% folate (2 mg/kg), 20% vitamin B_6 (6 mg/kg) and 10% choline (0.128 mg/kg) (VCDD)) and combined VCD/HCD. Special purified diets were acquired from Sniff, Germany. Average daily diet intake was determined by weighing the remaining food after two days once per week for each animal. Weight was measured once a week. Six or eight weeks later, rabbits were sacrificed and the aortas dissected. Same sections were used for myography, MRI and other analyses. All specimens from myography and MRI were used for histology.

2.3. Vessel wall injury

Injury of the adult rabbit aorta abdominalis was performed by three techniques: the automated JURY-controlled injury, classical “blind” injury without pressure monitoring and manual pressure-adjusted injury (a modification of classical “blind” injury with monitoring and manual adjustment of the pressure). A detailed description of the JURY device and the surgery is provided in supplement 1 and 2.

- ***Classical “blind” injury****:* manual injury, during which the pressure is regulated manually by thumb press on a syringe; no display of pressure data for the operator; manual retraction with undefined speed. To compare pressure curve in classical “blind” injury with pressure curves in manual pressure-adjusted injury and JURY-controlled injury the catheter during classical “blind” injury was connected to a 1 ml Luer-Lock syringe and the JURY device with a pressure sensor in between. Only during the inflation of the balloon the operator was informed by the assistant when the target pressure was reached, otherwise the operator could only maintain the pressure according to his feeling (“blind”).

- ***Manual pressure-adjusted injury****:* a modification of the classical “blind” injury with monitoring and manual adjustment of the pressure by the operator based on the displayed pressure curve; manual retraction with undefined speed. The catheter was connected to a 1 ml Luer-Lock syringe and the JURY device with a pressure sensor in between. The balloon pressure was displayed on a computer monitor in real-time.

- ***JURY-controlled injury****:* fully automated JURY-controlled injury with pressure being displayed, recorded and adjusted automatically, JURY-controlled retraction with preset speed. For this technique the catheter is locked to a pressure sensor (Pendotech, USA) on a 1 ml Luer-Lock syringe that is firmly clamped to the sled of the JURY device (Fig. S2). The desired target pressure and the retraction speed are entered in the graphical user interface of the JURY controller software (Arduino, USA). After reaching the target pressure, which takes a few seconds, the retraction of the catheter is initiated. After reaching the desired end position, the balloon is deflated and the catheter is gently removed. Initiated by the operator, balloon inflation, retraction at constant pressure and constant speed as well as deflation are all performed automatically by the JURY device.

To compare the injury protocols described above 3 NZW rabbits were used. In the first animal, the operator performed the balloon injury “blind” without monitoring the pressure curve. In the second animal, the operator monitored the pressure curve during the denudation and manually adjusted the pressure to 1.8 bar. The catheter was retracted manually (undefined speed) in the first and second animal. In the third animal, the JURY device was pre-adjusted to maintain a pressure of 1.8 bar and a constant retraction speed of 5 mm/s. In all cases, pressure and, if applicable, motor step data were recorded by the JURY device in real-time. The comparison of the methods is shown in Fig. 1. Due to high variation in the target pressure, the classical “blind” injury protocol was not further used.

Subsequently, abdominal aortas were injured in 6 NZW rabbits at a target pressure of 1.2 bar (minimal pressure for inflating the balloon) and a single retraction: 3 rabbits were treated according to the manual pressure-adjusted injury protocol and 3 rabbits according to the automated JURY-controlled injury protocol (constant retraction speed of 5 mm/s). Aortas from two untreated rabbits were used as controls. The following day, rabbits were sacrificed and the aorta abdominalis dissected in the area of the denudation to assess the injury.

In the next step, atherosclerotic plaque formation was examined in rabbit groups of 4-6 (NZW rabbits and cbHyla). Aortas were injured by manual pressure-adjusted or JURY-controlled injury techniques. The

injury conditions used were either 1.2 bar (mild injury: minimal pressure; 1x pull-back) or 1.8 bar (severe injury: higher pressure; 3x pull-backs). After the injury, all rabbits were fed HCD for 6 weeks.

NZW rabbits were used to compare the effects of the modified diets on atherosclerotic transformation of the aorta. The rabbits were divided into 4 groups of 8 animals each. All vessel wall injuries were performed automatically with one retraction by the JURY device at 1.8 bar and a 60% reduced retraction speed of 2 mm/s to intensify single-applied injury. In the HCD, VCDD and VCD/HCD groups, the animals were preconditioned before the surgery (VCDD was initiated two weeks and HCD one week before vessel wall injury). One day after the injury, the special diets were resumed and fed for additional 8 weeks.

2.4. Plasma Hcy, total cholesterol and triglyceride levels

Methanol (MeOH), water (MS-grade) and acetonitrile were purchased from Merck, USA. 1,4-dithiothreitol (DTT), trifluoroacetic anhydride and ammonium acetate were purchased from Sigma, USA. Formic acid was purchased from Roth, Germany. L-Hcy from Sigma was used as the standard. DL-Hcy-d4 from CDN isotopes, Canada was used as an internal standard. All standard stock solutions were prepared in H_2O + 0.1% formic acid and stored at -80°C until use. Blood was taken from the ear vein or by heart puncture after sacrifice, collected into EDTA or Lithium Heparin Vacuette® tubes (Greiner, Germany) and centrifuged for 15 min at 4°C and 3,200 rpm. Blood plasma was immediately aliquoted and frozen at -80°C. In order to analyse the plasma Hcy levels, 100 µl of each plasma sample were mixed with 25 µl of 20 mmol/l DL-Hcy-d4 as internal standard and 10 µl of 0.5 mol/l DTT and incubated for 15 min at RT. Then 300 µl of precipitation reagent (acetonitrile + 0.1% formic acid + 0.05% trifluoroacetic acid) were added, the samples were centrifuged for 5 min at 13,000 rpm at room temperature (RT) and 125 µl of the supernatant were transferred into an autosampler vial. The solvent was then evaporated for about 30-45 min under a stream of nitrogen and the samples were reconstituted in 125 µl of H_2O/MeOH 9:1 (v/v) + 0.1% formic acid. For the absolute quantification of Hcy in the plasma, a dilution series for a calibration curve in the range from 1.4138 to 113.1034 µmol/l Hcy was prepared, followed by the preparation of quality controls (QC) at 94.25 µmol/l, 11.31 µmol/l and 1.885 µmol/l Hcy. Plasma Hcy levels were analyzed using a 1290 Infinity UHPLC coupled to a 6470 Triple-Quadrupole mass spectrometer (Agilent, USA) using a BEH C_{18} column (3.0 mm x 150 mm; 1.7 µm) (Waters, USA) with 50°C column temperature, 5 µl injection volume and a constant flow rate of 200 µl/min under the control of Agilent MassHunter Workstation Data Acquisition software. H_2O + 0.1% formic acid (A) and methanol + 0.1% formic acid (B) were used as solvents. 95% solvent A was held for 2 min, followed by a change to 100% solvent B over the next 2 min, which was held for an additional 3.5 min. Re-equilibration was carried out by changing to 95% solvent A within 5 seconds, followed by 3 min at 95% solvent A. Total running time was 11 min. Hcy and Hcy-d4 as internal standards were analyzed in the MRM mode. The dwell time for all transitions was 60 ms, the fragmentor voltage 80 and the cell acceleration voltage 4. The transitions m/z 136 to 90 for

Hcy and m/z 140 to 94 for Hcy-d4, both with a collision energy of 15, were used as quantifiers. The transitions m/z 136 to 73 and 56 were the qualifiers for Hcy, m/z 140 to 77 and 59 for Hcy-d4, respectively, all with a collision energy of 19. Plasma total cholesterol and triglyceride levels were analysed using a cobas 8000 modular routine analyser (Roche, Austria).

2.5. Lipoprotein analysis

Plasma from rabbits of each dietary group was pooled and diluted with PBS if necessary. 200 µl of each plasma pool was subjected to fast protein liquid chromatography (FPLC) on a Pharmacia FPLC system (Pfizer Pharma, Germany) equipped with a Superose 6 (30x1cm) column (Amersham Biosciences, USA). The lipoproteins were eluted with 10 mM Tris-HCl, 1 mM EDTA, 0.9% NaCl and 0.02% NaN_3 (pH 7.4) in fractions of 0.5 ml/min for 60 min. Total cholesterol and triglyceride concentrations were determined enzymatically. To enhance sensitivity, the reaction buffers were supplemented with sodium 3,5-dichloro-2-hydroxy-benzenesulfonate.

2.6. Biaxial extension tests

The biomechanical properties of the aortas were determined by biaxial strain tests of square-shaped aortic specimens with a side length of approx. 8 mm, the sides being aligned in the circumferential and axial directions of the aorta. The specimens were mounted to the carriages of the biaxial extension stage and immersed in a phosphate-buffered physiological solution (PBS) at 37°C. During testing, the specimens were subjected to various loading protocols in order to determine the physiological deformations of the tissue. Different stretches (1.1–1.6 in 0.1 increments) were applied consecutively, starting with the lowest stretch until the tissue failed. For each stretch level, four preconditioning cycles and one measuring cycle were performed with different loading ratios (1(circ.):1(axial), 1 : 0:75; 1 : 0:5; 0:75 : 1, 0:5 : 1) with an actuator speed of 3 mm/min. Each measuring cycle consists of a loading and an unloading path. It is crucial to use different load ratios between the circumferential and axial directions in order to cover the physiological deformations and to capture the direction-dependent material response of the aortas by means of biaxial extension tests. In addition, this so-called ‘true’ biaxial test approach results in a unique set of constitutive parameters for the specimen to be tested. The forces of load cells, positions of carriages and distances between special tissue markers (which act as gage markers) recorded by a videoextensometer were recorded continuously. Cauchy stress versus stretch ratio plots were generated from these data sets. The authors found that the results were very sensitive to the initial preloads. In order to obtain reproducible results, a prestress of about 0.1 kPa in terms of engineering stress (corresponds to 5 mN) was applied to each specimen.

2.7. Myography

Aortic rings were prepared from the abdominal aorta. The aortic segments were rapidly cleaned from the surrounding tissue, cut into 2 mm rings and transferred to the physiological buffer described below. The rings were mounted on pins connected to a micrometer and a force transducer. The experiments were carried out in myograph chambers (620M Multi Wire Myograph System; Danish MyoTechnology, Denmark) filled with a modified Krebs-Ringer bicarbonate buffer solution (KRS) consisting of 119 mM NaCl, 4.7 mM KCl, 1.2 mM KH_2PO_4, 1.2 mM $MgCl_2$, 2.5 mM $CaCl_2$, 25 mM $NaHCO_3$, 0.03 mM EDTA-Na_2 and 5.5 mM D-glucose. The rings were kept in an open bath at 37°C, while the KRS was continuously oxygenated with 95% O_2 and 5% CO_2 to keep the pH at 7.4. The maximal active tension was achieved by contracting the rings with the modified KRS with high K^+ concentration (65 mM NaCl, 59 mM KCl, 1.2 mM $MgSO_4$, 1.2 mM KH_2PO_4, 2.5 mM $CaCl_2$, 25 mM $NaHCO_3$, 0.03 mM EDTA-Na_2 and 5.5 mM D-glucose). After reaching maximal isometric tension, the high K^+ content was washed out and the rings were allowed to relax in a physiological buffer. The rings were then gradually contracted with increasing concentrations of norepinephrine (1 nM – 0.3 µM) to reach 80% of the maximum norepinephrine-induced contraction and then relaxed with increasing concentrations of acetylcholine chloride (1 nM – 0.3 µM) to assess endothelium-dependent relaxation. In order to examine endothelium-independent relaxation, the rings were washed and constricted with norepinephrine to 80% of the maximal constriction, and subsequently exposed to increasing concentrations of the nitric oxide donor sodium nitroprusside (0.1 nM – 30 nM). Relaxation values were expressed as a percentage of the norepinephrine-induced contraction.

2.8. MRI analysis

Evaluation of plaque area: For the assessment of plaque area a 5 cm piece of dissected aorta was washed with PBS (pH 7.4) and immersed in perfluoropolyether (Fomblin®, Solvay, Italy) in a 1 ml Luer-Lock syringe without air bubbles. Fomblin®, a contrast agent without MR signal, was added to minimize magnetic susceptibility effects at air-tissue boundaries (Clarke et al., 2003). The specimens were scanned with a 15.2 Tesla small animal MRI (Biospec 152/11, Bruker, Germany). For segmentation of the aortic sections, a proton density-weighted, fat-saturated 2D fast spin echo sequence with the following parameters was used: TR/TE = 1500/2.9 ms, turbo factor = 1, slice thickness = 500 µm, in-plane resolution = 100 µm x 100 µm, imaging matrix = 200 x 200, the number of segments was between 59 and 120 slices (Fig. 2). A slightly different setting was used to assess plaque area in rabbits fed different diets (Fig. 3). For the assessment of plaque area in rabbits fed different diets aortic sections of 1 cm in length were taken from approximately the same position from each animal and immersed in Fomblin®. A 7 Tesla small-animal scanner (Biospec 70/20, Bruker, Germany) equipped with a cryogenic cooled transceiver was used. A proton density-weighted, fat-saturated 2D fast spin echo sequence with the following parameters: TR/TE = 1900/6.64 ms, turbo factor = 2, slice thickness = 500 µm, in-plane resolution = 60 µm x 60 µm, imaging matrix = 200 x 200, 40 slices per aorta. For both studies, the mean

cross-sectional area of the vessel wall across the entire specimens was analyzed by semi-automated segmentation with a custom build tool created in Matlab (MathWorks Inc, USA).

Diffusion tensor MRI: Within the same imaging session, a fat-saturated segmented diffusion tensor imaging protocol was used with the key parameters: EPI readout with 4 segments, TR/TE = 2000/21.13 ms, slice thickness = 800 µm, in-plane resolution = 80 µm x 80 µm, imaging matrix = 128 x 128, 9 slices. Water diffusion was analyzed in 120 isotropically distributed directions at a b-value of 1000 s/mm². The average of 10 non-diffusion weighted scans was used as a reference for calibrating the diffusion tensor. Diffusion tensor images including fractional anisotropy maps of the aortic cross-sections were calculated with the software supplied with the MRI (Paravision 6.1, Bruker, Germany). After the scans, the syringes were emptied and refilled with PBS containing 4% paraformaldehyde (PFA) for preservation and later histological analysis.

2.9. Histology

For cryosectioning, the aortic rings were washed in PBS (pH 7.4), after MRI or myography, embedded in Tissue Tek O.C.T T COMPOUND (VWR International, Austria) and frozen at −20°C in a cryotom (Microm, Germany). Slices of 8 µm thickness were cut, transferred to SuperFrost® Plus glass slides (Thermo Scientific, Germany) and dried overnight.

For CD31 endothelial and RAM11 macrophage immunostaining, procedures were performed at RT using a Polink-2 Plus Mouse Detection System kit (GBI Labs, USA). The slides were rinsed twice with PBS (5 min each time) and blocked with sterile filtered PBS + 5% BSA for 30 min. The slides were then incubated with a mouse anti-human CD31 antibody (clone JC/70A, Abcam, UK) 1:20 dilution or an anti-rabbit RAM11 antibody (Dako/Agilent, USA) 1:50 dilution in PBS + 0.5% BSA, according to the Polink staining protocol. As substrate BCIP/NBT solution (GBI Labs, USA) was used as substrate and the slides were counterstained with filtered neutral red solution (1% acetic acetate in dH_2O, 10 mg/ml neutral red dye (Fluka Analytical, Switzerland) for 5 min. Finally, the slides were dried, and covered with Aquatex (Merck, USA) and a cover slip.

Oil red O neutral lipid staining was performed at RT. The slides were each rinsed with PBS, distilled water and 2-propanol solution (60% + 40% dH_2O) for 5 min. The slides were then stained in freshly prepared and filtered oil red O solution (60% 2-propanol, 40% dH_2O, 10 mg/ml oil red O dye, Sigma-Aldrich, USA) for 15 min, briefly de-stained with the same 2-propanol solution and washed in dH_2O. Finally, the slides were counterstained for nuclei with Haemalaun nach Mayer (Gatt-Koller, Austria) for 2 min, washed with dH_2O, dried, and covered with Aquadex (Merck, USA) and a cover slip. After drying, the slides were visualised in transmitted light mode of an Olympus BX51 Basic Fluorescence Microscope (Germany) with a DP71 camera. All images were taken with an UPlan Apo Infinity Corrected 4× objective. Liver tissue was fixed in PBS pH 7.4 + 4% PFA, embedded in paraffin blocks, and 3 µm sections were cut using a microtome

(Histocom, Micron HM440E, Switzerland). The sections were stained with hematoxylin and eosin according to standard protocols.

2.10. Sample preparation and multi-photon microscopy

Ring-like pieces of rabbit aortas were cut longitudinally under the stereomicroscope using racer blades and subsequently mounted between two coverslips so that the aortic intima was flat to the objective. Imaging was performed at the IMB-Graz Optical Imaging Resource using a picosecond laser (picoEmerald; APE, Germany) integrated in a Leica SP5 confocal microscope (Leica Microsystems, Germany). The laser delivers temporally and spatially overlapping pulse trains: a stable 1064 nm line, a tunable signal beam and an idler beam. For coherent anti-Stokes Raman scattering (CARS) imaging of densely packed neutral lipids in lipid droplets, the signal beam was tuned to 816.4 nm (2840 cm^{-1}). The sample was illuminated simultaneously with the 1064 nm line, which led to the CARS signal of symmetrical CH_2 stretching vibrations of esterified fatty acids in lipid droplets. For second harmonic generation (SHG) imaging of collagen, the signal beam was tuned to 880 nm. A two-channel, non-descanned detector (NDD) in epi-mode was used to detect CARS and SHG signals simultaneously. An SP 680 barrier filter (excitation light filter), an RSP 495 beamsplitter for two-channel separation of emitted light towards a 465/120 (‘SHG channel’) and a 650/210 (‘CARS channel’) bandpass filter was used. The wide range of the bandpass filters allows the additional detection of two-photon excited autofluorescence (TPAF) mainly of elastin in the ‘CARS channel’ and of elastin and cellular structures in the ‘SHG channel.’ The SHG signal from collagen and the CARS signal from lipid droplets were typically significantly stronger than the autofluorescence signal from elastin and cellular structures under the same imaging conditions. Optical sections were acquired using HCX IRAPO L 25× NA 0.95 water immersion and a sampling interval of 125 nm x 125 nm. Eight- to sixteen-times line averaging was applied to reduce image noise.

2.11. Electron microscopy

Aortic tissue was fixed in 2.5% (w/v) glutaraldehyde and 2% PFA (w/v) in 0.1 M cacodylate buffer, pH 7.4, for 2 h, and then post-fixed in 2% (w/v) osmium tetroxide for 2 h at room temperature (RT). After dehydration (in graded series of ethanol), tissues were infiltrated (ethanol and TAAB Embedding Resin, pure TAAB Embedding Resin) and placed in TAAB Embedding Resin (8 h), transferred into embedding moulds, and polymerised (48 h, 60°C). Ultrathin sections (70 nm) were cut with a UC 7 Ultramicrotome (Leica Microsystems, Austria) and stained with lead citrate for 5 min and platinum blue for 15 min. Electron micrographs were taken using a Tecnai G2 transmission electron microscope (FEI, Netherlands) with a Gatan Ultrascan 1000 charge coupled device (CCD) camera (-20°C, acquisition software Digital Micrograph, Gatan, Germany and Serial EM). Acceleration voltage was 120 kV.

2.12. Statistical analysis

Data are presented as line graphs or as box plots partially with single data points superimposed (e.g. vessel wall area), respectively. Indicated sample sizes in figure legends refer to biological replicates (independent animals). Comparisons between two groups were done by Mann Whitney U test, if data violating normality distribution. In case of multiple group comparisons, analysis of variance (ANOVA) or Kruskal-Wallis test followed by Bonferroni post hoc tests were applied. In case of serial measurements (concentration), Greenhouse-Geisser–corrected two-way repeated-measures ANOVA was used. Generally, significant factorial designs were followed by pairwise comparisons that were corrected in case of multiple comparisons by Bonferroni post hoc analyses. Data residual distribution was confirmed by Shapiro-Wilk's test and visual data inspection by use of Q-Q plots, whereas homogeneity of variance was verified by Levene's test. All reported P values are two-sided, and an a level of 0.05 was used throughout. Analyses were performed with SPSS 27.0 (SPSS Inc., Chicago, USA) or GraphPad Prism 8 (GraphPad Software LLC, Massachusetts, USA). The statistical analysis is shown in S7.

Abbreviations

SD – standard diet, HCD – high cholesterol diet, VCDD – vitamin and choline deficient diet, VCD/HCD - vitamin and choline deficient high cholesterol diet, Hcy – homocysteine, HHcy – hyperhomocysteinemia, LDL – low density lipoprotein, VLDL – very low density lipoprotein, MRI – magnetic resonance imaging, FA – fractional anisotropy, SHG – second harmonic generation, TPAF – two-photon excited autofluorescence, CARS – coherent anti-Stokes Raman scattering

Declarations

Acknowledgements

We would like to especially thank Brigitte Spreitzer for helping with animal experiments and technical assistance in sample preparation. Special thanks go to Dr. phil. Univ.-Prof. Günther Jürgens for his great help and support in the initial phase of this work. We would like to thank Anton Ibovnik, Christina Bachmayer, Peter Daringer, Anton Lienbacher, Markus Oberndorfer, Kerstin Hingerl and Dominique Pernitsch for the technical support.

Sources of funding

This work was funded by the EU project NanoAthero, by the Austrian Science Fund (FWF) (Projects P31105 and P33672), and BioTechMed-Graz Future Space.

Author contributions

Gunter Almer – animal study, histology, contribution to design, interpretation and discussion of results, writing of paper

Peter Opriessnig – MRI, interpretation and discussion of results

Heimo Wolinski – SHG/TPAF, CARS, interpretation and discussion of results

Gerhard Sommer – biomechanical testing, interpretation and discussion of results

Margarete Lechleitner –myography

Clemens Diwoky – MRI, interpretation and discussion of results

Dagmar Kolb – electron microscopy, interpretation and discussion of results

Vladimir Bubalo – surgery, balloon injury

Markus S. Brunner – Hcy plasma levels

Andreas N. Schwarz – data analysis

Gerd Leitinger – electron microscopy, interpretation and discussion of results

Gabriele Schoiswohl – contribution to design of animal study, interpretation and discussion of results

Gunther Marsche – contribution to design of animal study, interpretation and discussion of results

Tobias Niedrist – plasma total cholesterol and triglyceride measurements

Silvia Schauer – liver histology

Wolfgang Oswald – contribution to design of animal study

Andrea Groselj-Strele – statistical analysis

Margret Paar – contribution to design of balloon injury study

Gerhard Cvirn – contribution to design of balloon injury study

Gerald Hoefler – pathological examination, liver histology

Gerald N. Rechberger – Hcy analytics, contribution to design of animal study, interpretation and discussion of results, writing of paper

Markus Herrmann - animal study

Saša Frank – myography, contribution to design of balloon injury and animal study, interpretation and discussion of results

Gerhard A. Holzapfel – biomechanical testing, interpretation and discussion of results, writing of paper

Dagmar Kratky – lipoprotein analysis, contribution to design of animal study, interpretation and discussion of results, writing of paper

Harald Mangge – background of atherosclerosis and cardiovascular diseases, animal study

Gerd Hörl*– conceiving of balloon injury study, balloon injury, interpretation and discussion of results, writing of paper

Oksana Tehlivets*– conceiving of diet study, statistical analysis, interpretation and discussion of results, writing of paper

Competing interest statements

The authors of the manuscript declare no conflicts of interests.

References

AL-MUSHARAF, S., ALJURAIBAN, G. S., DANISH HUSSAIN, S., ALNAAMI, A. M., SARAVANAN, P. & AL-DAGHRI, N. 2020. Low Serum Vitamin B12 Levels Are Associated with Adverse Lipid Profiles in Apparently Healthy Young Saudi Women. *Nutrients,* 12.

ASADA, Y., KISANUKI, A., TSUNEYOSHI, A., MARUTSUKA, K., HATAKEYAMA, K. & SUMIYOSHI, A. 1996. Effects of inflation pressure of balloon catheter on vascular injuries and subsequent development of intimal hyperplasia in rabbit aorta. *Atherosclerosis,* 121**,** 45-53.

CECELJA, M. & CHOWIENCZYK, P. 2012. Role of arterial stiffness in cardiovascular disease. *JRSM Cardiovasc Dis,* 1.

CHEN, J. Z., SAWADA, H., MOORLEGHEN, J. J., WEILAND, M., DAUGHERTY, A. & SHEPPARD, M. B. 2019. Aortic Strain Correlates with Elastin Fragmentation in Fibrillin-1 Hypomorphic Mice. *Circ Rep,* 1**,** 199-205.

CLARKE, S. E., HAMMOND, R. R., MITCHELL, J. R. & RUTT, B. K. 2003. Quantitative assessment of carotid plaque composition using multicontrast MRI and registered histology. *Magn Reson Med,* 50**,** 1199-208.

COOLEN, B. F., CALCAGNO, C., VAN OOIJ, P., FAYAD, Z. A., STRIJKERS, G. J. & NEDERVEEN, A. J. 2018. Vessel wall characterization using quantitative MRI: what's in a number? *MAGMA,* 31**,** 201-222.

DONG, X., YAO, Z., HU, Y., YANG, N., GAO, X., XU, Y. & WANG, G. 2016. Potential harmful correlation between homocysteine and low-density lipoprotein cholesterol in patients with hypothyroidism. *Medicine,* 95**,** e4291.

GETZ, G. S. & REARDON, C. A. 2006. Diet and murine atherosclerosis. *Arterioscler Thromb Vasc Biol,* 26**,** 242-9.

HOFMANN, M. A., LALLA, E., LU, Y., GLEASON, M. R., WOLF, B. M., TANJI, N., FERRAN, L. J., JR., KOHL, B., RAO, V., KISIEL, W., STERN, D. M. & SCHMIDT, A. M. 2001. Hyperhomocysteinemia enhances vascular inflammation and accelerates atherosclerosis in a murine model. *J Clin Invest,* 107**,** 675-83.

HUBMACHER, D., CIRULIS, J. T., MIAO, M., KEELEY, F. W. & REINHARDT, D. P. 2010. Functional consequences of homocysteinylation of the elastic fiber proteins fibrillin-1 and tropoelastin. *J Biol Chem,* 285**,** 1188-98.

IP, J. H., FUSTER, V., BADIMON, L., BADIMON, J., TAUBMAN, M. B. & CHESEBRO, J. H. 1990. Syndromes of accelerated atherosclerosis: role of vascular injury and smooth muscle cell proliferation. *J Am Coll Cardiol,* 15**,** 1667-87.

KARGER, A. B., STEFFEN, B. T., NOMURA, S. O., GUAN, W., GARG, P. K., SZKLO, M., BUDOFF, M. J. & TSAI, M. Y. 2020. Association Between Homocysteine and Vascular Calcification Incidence, Prevalence, and Progression in the MESA Cohort. *J Am Heart Assoc,* 9**,** e013934.

LEFKOWITZ, R. J. & WILLERSON, J. T. 2001. Prospects for cardiovascular research. *JAMA,* 285**,** 581-7.

LIANG, C., WANG, Q. S., YANG, X., ZHU, D., SUN, Y., NIU, N., YAO, J., DONG, B. H., JIANG, S., TANG, L. L., LOU, J., YU, C. J., SHAO, Q., WU, M. M. & ZHANG, Z. R. 2021. Homocysteine Causes Endothelial Dysfunction via Inflammatory Factor-Mediated Activation of Epithelial Sodium Channel (ENaC). *Front Cell Dev Biol,* 9**,** 672335.

LIBBY, P. 2021. The changing landscape of atherosclerosis. *Nature,* 592**,** 524-533.

MIKAEL, L. G., GENEST, J., JR. & ROZEN, R. 2006. Elevated homocysteine reduces apolipoprotein A-I expression in hyperhomocysteinemic mice and in males with coronary artery disease. *Circ Res,* 98**,** 564-71.

NISHIGA, M., WANG, D. W., HAN, Y., LEWIS, D. B. & WU, J. C. 2020. COVID-19 and cardiovascular disease: from basic mechanisms to clinical perspectives. *Nat Rev Cardiol,* 17**,** 543-558.

OPRIESSNIG, P., MANGGE, H., STOLLBERGER, R., DEUTSCHMANN, H. & REISHOFER, G. 2016. In vivo cardiovascular magnetic resonance of 2D vessel wall diffusion anisotropy in carotid arteries. *J Cardiovasc Magn Reson,* 18**,** 81.

PERLA-KAJAN, J., UTYRO, O., RUSEK, M., MALINOWSKA, A., SITKIEWICZ, E. & JAKUBOWSKI, H. 2016. N-Homocysteinylation impairs collagen cross-linking in cystathionine beta-synthase-deficient mice: a novel mechanism of connective tissue abnormalities. *FASEB J,* 30**,** 3810-3821.

PHINIKARIDOU, A., HALLOCK, K. J., QIAO, Y. & HAMILTON, J. A. 2009. A robust rabbit model of human atherosclerosis and atherothrombosis. *J Lipid Res,* 50**,** 787-97.

REFSUM, H., UELAND, P. M., NYGARD, O. & VOLLSET, S. E. 1998. Homocysteine and cardiovascular disease. *Annu Rev Med,* 49**,** 31-62.

SELHUB, J. 2006. The many facets of hyperhomocysteinemia: studies from the Framingham cohorts. *J Nutr,* 136**,** 1726S-1730S.

SELHUB, J., JACQUES, P. F., WILSON, P. W., RUSH, D. & ROSENBERG, I. H. 1993. Vitamin status and intake as primary determinants of homocysteinemia in an elderly population. *JAMA,* 270**,** 2693-8.

TAMURA, Y., SHIMOJI, K., ISHIKAWA, J., MATSUO, Y., WATANABE, S., TAKAHASHI, H., ZEN, S., TACHIBANA, A., OMURA, T., KODERA, R., OBA, K., TOYOSHIMA, K., CHIBA, Y., TOKUMARU, A. M. & ARAKI, A. 2021. Subclinical Atherosclerosis, Vascular Risk Factors, and White Matter Alterations in Diffusion Tensor Imaging Findings of Older Adults With Cardiometabolic Diseases. *Front Aging Neurosci,* 13**,** 712385.

TENG, Y. W., CERDENA, I. & ZEISEL, S. H. 2012. Homocysteinemia in mice with genetic betaine homocysteine S-methyltransferase deficiency is independent of dietary folate intake. *J Nutr,* 142**,** 1964-7.

TORNIFOGLIO, B., STONE, A. J., JOHNSTON, R. D., SHAHID, S. S., KERSKENS, C. & LALLY, C. 2020. Diffusion tensor imaging and arterial tissue: establishing the influence of arterial tissue microstructure on fractional anisotropy, mean diffusivity and tractography. *Sci Rep,* 10**,** 20718.

VACEK, T. P., REHMAN, S., NEAMTU, D., YU, S., GIVIMANI, S. & TYAGI, S. C. 2015. Matrix metalloproteinases in atherosclerosis: role of nitric oxide, hydrogen sulfide, homocysteine, and polymorphisms. *Vasc Health Risk Manag,* 11**,** 173-83.

VAN DER DONCKT, C., VAN HERCK, J. L., SCHRIJVERS, D. M., VANHOUTTE, G., VERHOYE, M., BLOCKX, I., VAN DER LINDEN, A., BAUTERS, D., LIJNEN, H. R., SLUIMER, J. C., ROTH, L., VAN HOVE, C. E., FRANSEN, P., KNAAPEN, M. W., HERVENT, A. S., DE KEULENAER, G. W., BULT, H., MARTINET, W., HERMAN, A. G. & DE MEYER, G. R. 2015. Elastin fragmentation in atherosclerotic mice leads to intraplaque neovascularization, plaque rupture, myocardial infarction, stroke, and sudden death. *Eur Heart J,* 36**,** 1049-58.

VERMEULEN, E. G., STEHOUWER, C. D., TWISK, J. W., VAN DEN BERG, M., DE JONG, S. C., MACKAAY, A. J., VAN CAMPEN, C. M., VISSER, F. C., JAKOBS, C. A., BULTERJIS, E. J. & RAUWERDA, J. A. 2000. Effect of homocysteine-lowering treatment with folic acid plus vitamin B6 on progression of subclinical atherosclerosis: a randomised, placebo-controlled trial. *Lancet,* 355**,** 517-22.

VESELI, B. E., PERROTTA, P., DE MEYER, G. R. A., ROTH, L., VAN DER DONCKT, C., MARTINET, W. & DE MEYER, G. R. Y. 2017. Animal models of atherosclerosis. *Eur J Pharmacol,* 816**,** 3-13.

VISRAM, M., RADULOVIC, M., STEINER, S., MALANOVIC, N., EICHMANN, T. O., WOLINSKI, H., RECHBERGER, G. N. & TEHLIVETS, O. 2018. Homocysteine regulates fatty acid and lipid metabolism in yeast. *J Biol Chem*, 293, 5544-5555.

VOLLSET, S. E., REFSUM, H., TVERDAL, A., NYGARD, O., NORDREHAUG, J. E., TELL, G. S. & UELAND, P. M. 2001. Plasma total homocysteine and cardiovascular and noncardiovascular mortality: the Hordaland Homocysteine Study. *Am J Clin Nutr,* 74**,** 130-6.

WANG, H., JIANG, X., YANG, F., GAUBATZ, J. W., MA, L., MAGERA, M. J., YANG, X., BERGER, P. B., DURANTE, W., POWNALL, H. J. & SCHAFER, A. I. 2003. Hyperhomocysteinemia accelerates atherosclerosis in cystathionine beta-synthase and apolipoprotein E double knock-out mice with and without dietary perturbation. *Blood,* 101**,** 3901-7.

WERSTUCK, G. H., LENTZ, S. R., DAYAL, S., HOSSAIN, G. S., SOOD, S. K., SHI, Y. Y., ZHOU, J., MAEDA, N., KRISANS, S. K., MALINOW, M. R. & AUSTIN, R. C. 2001. Homocysteine-induced endoplasmic reticulum stress causes dysregulation of the cholesterol and triglyceride biosynthetic pathways. *J Clin Invest,* 107**,** 1263-73.

XU, R., HUANG, F., WANG, Y., LIU, Q., LV, Y. & ZHANG, Q. 2020. Gender- and age-related differences in homocysteine concentration: a cross-sectional study of the general population of China. *Sci Rep,* 10**,** 17401.

YAMASHITA, A., FURUKOJI, E., MARUTSUKA, K., HATAKEYAMA, K., YAMAMOTO, H., TAMURA, S., IKEDA, Y., SUMIYOSHI, A. & ASADA, Y. 2004. Increased vascular wall thrombogenicity combined with reduced blood flow promotes occlusive thrombus formation in rabbit femoral artery. *Arterioscler Thromb Vasc Biol,* 24**,** 2420-4.

YAN, Y., WU, X., WANG, P., ZHANG, S., SUN, L., ZHAO, Y., ZENG, G., LIU, B., XU, G., LIU, H., WANG, L., WANG, X. & JIANG, C. 2020. Homocysteine promotes hepatic steatosis by activating the adipocyte lipolysis in a HIF1alpha-ERO1alpha-dependent oxidative stress manner. *Redox Biol,* 37**,** 101742.

YIDENG, J., ZHIHONG, L., JIANTUAN, X., JUN, C., GUIZHONG, L. & SHUREN, W. 2008. Homocysteine-mediated PPARalpha,gamma DNA methylation and its potential pathogenic mechanism in monocytes. *DNA Cell Biol,* 27**,** 143-50.

ZULLI, A., WIDDOP, R. E., HARE, D. L., BUXTON, B. F. & BLACK, M. J. 2003. High methionine and cholesterol diet abolishes endothelial relaxation. *Arterioscler Thromb Vasc Biol,* 23**,** 1358-63.

Figures

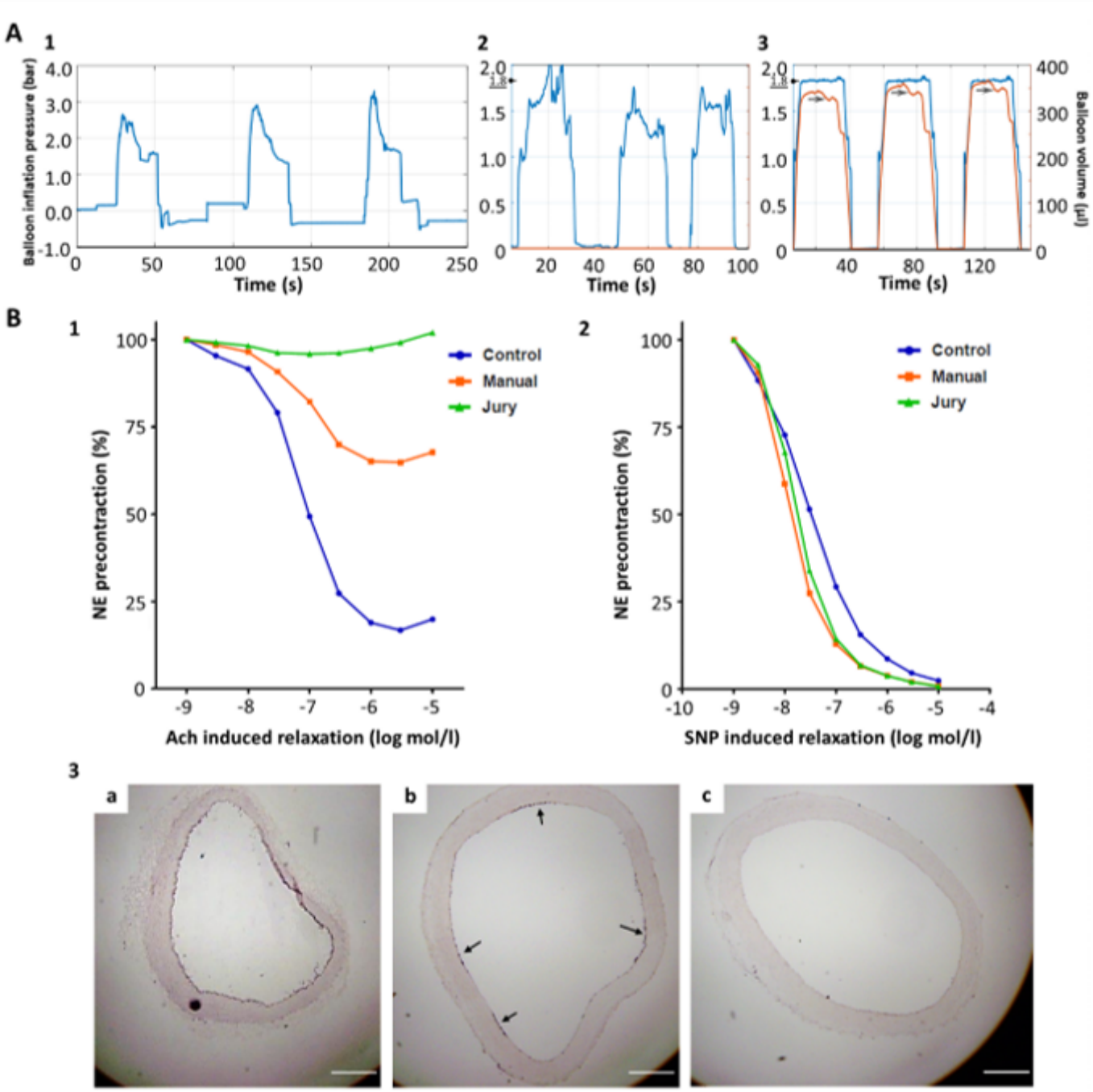

Figure 1

Development of JURY-controlled balloon injury technique. A Comparison of three vessel wall injury techniques. One rabbit per condition underwent vessel wall injury of the aorta abdominalis at a target pressure of 1.8 bar. Real-time pressure curves of three injury cycles (inflation-retraction-deflation) are shown. Black round arrows mark target pressure. Grey arrows mark reduction of balloon volume due to aorta narrowing. **A1** Classical “blind” injury: no pressure monitoring and adjustment, manual retraction, pressure was recorded by JURY for comparison with other techniques **A2** Modification of the classical “blind” injury - manual pressure-adjusted injury: pressure was manually adjusted by the operator based on pressure curve monitoring, manual retraction. **A3** Fully automated injury: JURY-controlled pre-adjusted pressure, JURY-controlled pre-adjusted retraction. Balloon volume is shown in µl. **B Effects of JURY-**

controlled and manual pressure-adjusted injury on endothelium under mild injury conditions. Three rabbits per condition underwent surgical intervention. Vessel wall injuries were performed at minimal balloon inflation pressure of 1.2 bar with single retraction. The next day, rabbits were sacrificed and the abdominal aorta dissected at the area of denudation. Two untreated rabbits were used as control. Shown is the relaxation of freshly dissected aortic sections, repeated measurements (in total 6-8 per rabbit) with (**B1**) acetylcholine (Ach) and (**B2**) sodium nitroprusside (SNP) after precontraction with norepinephrine (NE). **B3** Immunohistological staining of endothelial cells (CD31) of (**B3a**) untreated control aorta with intact endothelial layer, (**B3b**) aorta injured by manual pressure-adjusted technique with partially denuded endothelial layer (black arrows indicate intact endothelial areas) and (**B3c**) aorta automatically injured using the JURY device with completely denuded endothelial layer. Images are representative for each group. Bars, 500 µm. Significant differences are shown in S7.

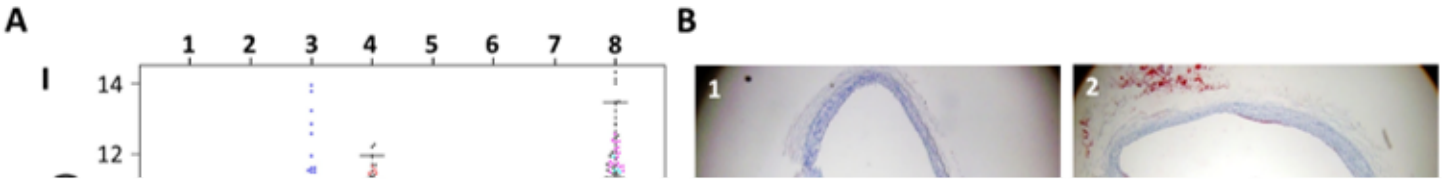

Figure 2

Atherosclerotic plaque development in two rabbit strains injured by JURY-controlled (J) vs manual pressure-adjusted technique (M). Groups of 4-6 animals (NZW (column 1-5) and cbHyla rabbits (column 6-8)) were injured either one time at minimum pressure of 1.2 bar (**A** condition 2, 3 and 6) or three times at 1.8 bar (**A** condition 4, 5, 7 and 8) either manually (M) or with the JURY device (J) at a retraction speed of 5 mm/s. A single untreated NZW rabbit (**A** column 1) served as a reference and was not used in statistical evaluations. After 6 weeks of HCD animals were sacrificed and aortas dissected. **A MRI analysis** of vessel wall area **(AI)** and fractional anisotropy **(AII)** of aortas from rabbits injured by JURY-controlled vs manual pressure-adjusted technique**.** Individual measuring points for each rabbit per group can be distinguished by the respective colors. Bold lines of boxes represent medians. *p<0.05; **p<0.01; ***p<0.001. **B Comparative histology of aortic specimens** (image index numbers correspond to conditions displayed in **A**). Identical aortic sections were cut into 8 smaller rings for cryo-sectioning and stained with oil red O (red) for neutral lipids and hematoxylin (blue) for cell nuclei. Images are representative for each group. Bars, 500 µm. Significant differences are shown in S7.

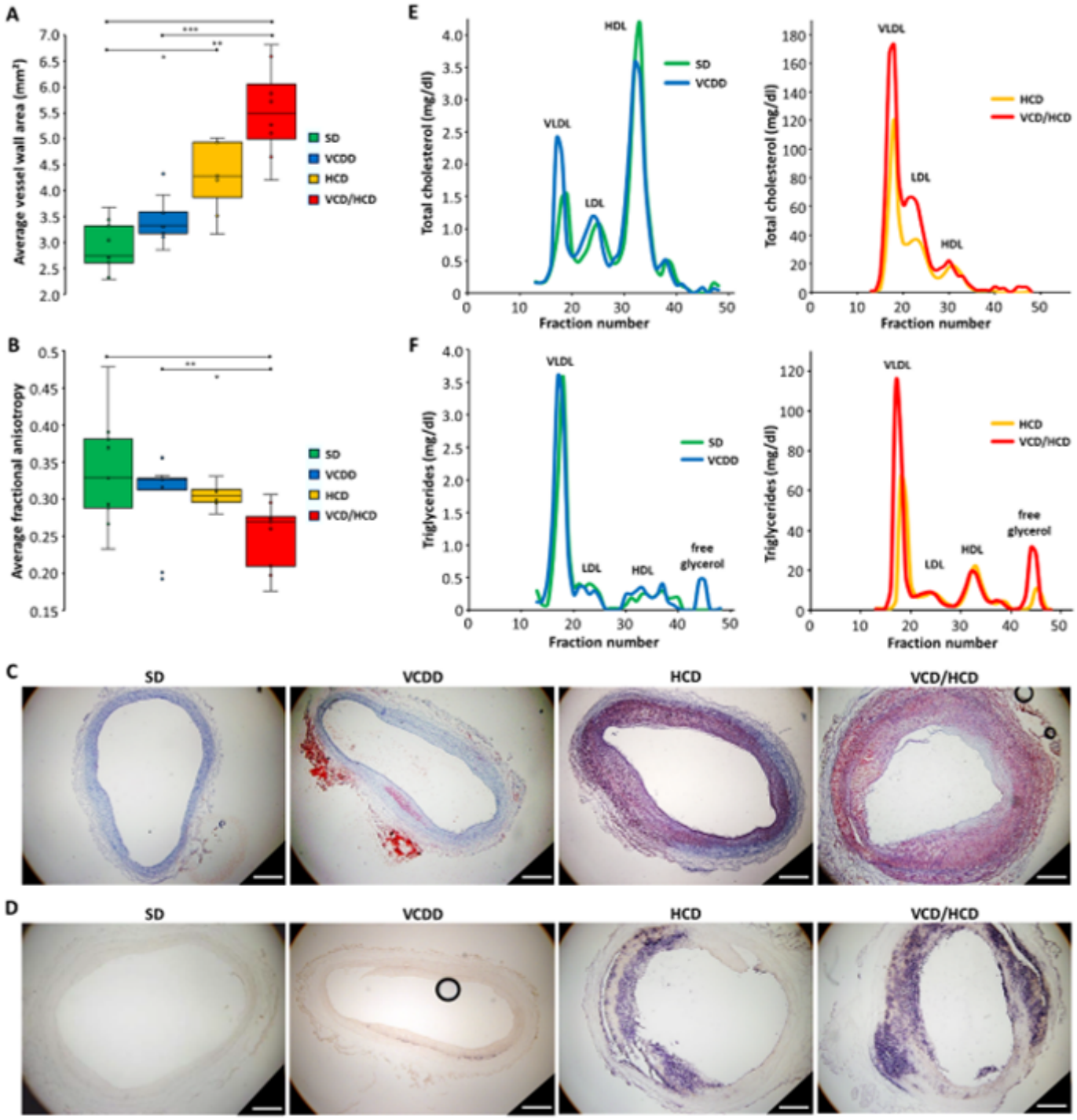

Figure 3

Atherosclerotic plaque development in JURY-injured aortas from rabbits fed different diets. Groups of 8 NZW rabbits were fed different diets and subjected to automated JURY-controlled injury at a pressure of 1.8 bar, single retraction and a 60% reduced retraction speed of 2 mm/s to intensify single-applied injury. VCDD was initiated two weeks and HCD one week before vessel wall injury for preconditioning. After 8 weeks post injury animals were sacrificed and aortas dissected. **A-B MRI analysis** of average vessel wall area **(A)** and fractional anisotropy **(B). C-D Representative histological sections** stained with oil red O (red) for neutral lipids and hematoxylin (blue) for cell nuclei **(C)**, and anti-rabbit RAM11 antibody (purple) for

macrophages and neutral red (background) **(D). E-F Lipoprotein profile** of total cholesterol **(E)** and triglycerides **(F**) after fast protein liquid chromatography separation in pooled plasma samples, (n=3-4). *P<0.05; **P<0.01; ***P<0.001. Bars, 500 µm. Significant differences are shown in S7.

Figure 4

Second harmonic generation (SHG) and anti-Stokes Raman scattering (CARS) microscopy of aortic sections from rabbits fed different diets. A Collagen/elastin organization and lipid droplet accumulation. Representative images of collagen/elastin fiber organization (SHG/TPA) in top panel and lipid accumulation (CARS/TPAF) in middle panel in the aortic intima are shown. Autofluorescence in response to VCD/HCD is most likely derived from dead/compromised macrophages. **B Accumulation of lipids and putative macrophages at the surface of the intima**, representative images. Autofluorescence is most likely due to an accumulation of cell bodies (SHG/TPAF) and lipid droplets (CARS/TPAF). Collagen/elastin fibers were not detected in **B**. Bars, 30 µm.

Figure 5

Representative transmission electron micrographs from aortic media of rabbits fed different diets. A1-4 SD. Elastic fibers (ef) appear continuous, smooth muscle cells (sm) are in close proximity, fibroblasts (f) and surrounding collagen fibers (cf) appear normal. Smooth muscle cells are recognized by their dense bodies (arrowhead in **A4**). **B1-4 VCDD.** Elastic fibers (ef) appear continuous, smooth muscle cells (sm) contain lipid droplets (asterisk). Fibroblasts (f) also indicate high amount of lipid droplets (asterisk) and dilated endoplasmic reticulum (arrow). **C1-4 HCD.** Elastic fibers (ef) are continuous, both smooth muscle cells (sm) and fibroblasts (f) contain lipid droplets (asterisks) and are surrounded by collagen fibers (cf). **D1-4 VCD/HCD.** The spacing between elastic fibers (ef) is widened. Smooth muscle cells (sm) and fibroblasts (f) exhibit an accumulation of lipid droplets (asterisks) and dilated endoplasmic reticulum (arrow) respectively. Some putative smooth muscle fiber structures are swollen and void of compartments (void profiles, vp). Bars, 5 µm.

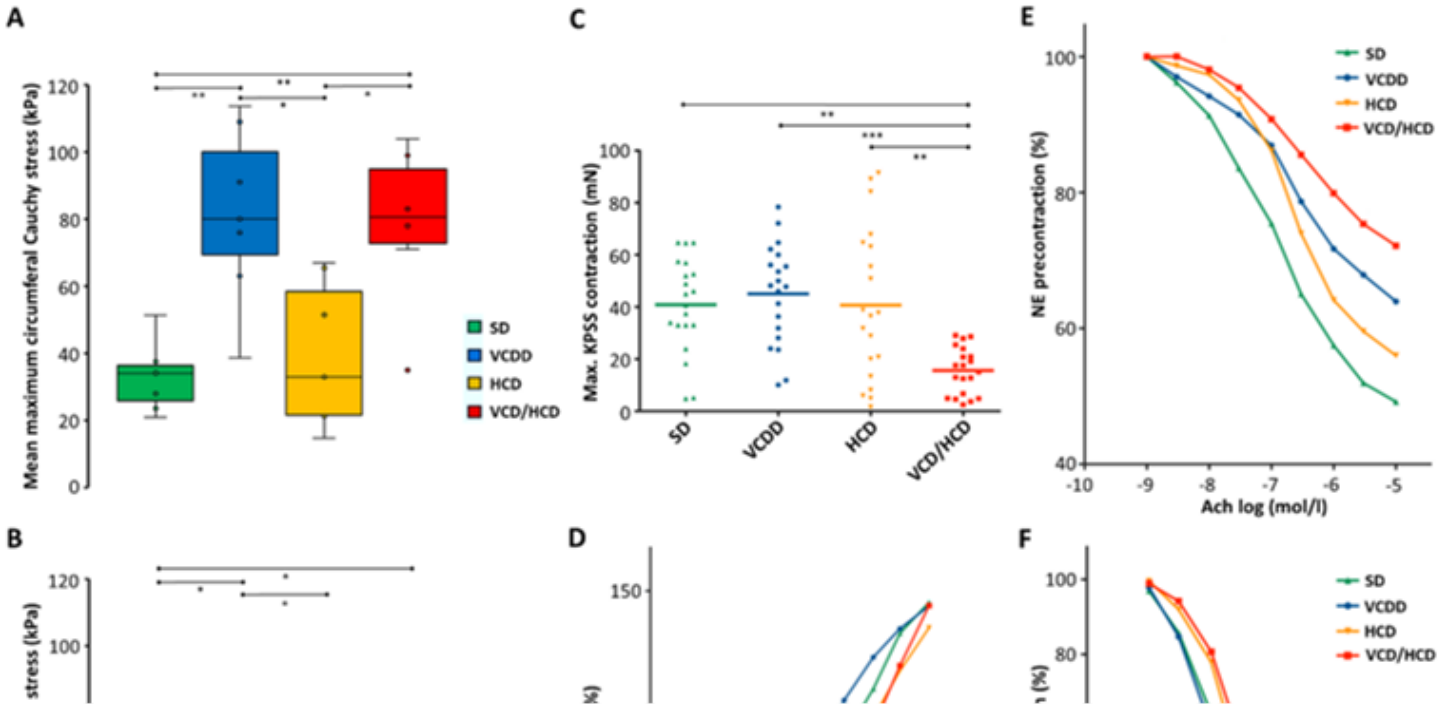

Figure 6

Biomechanical properties and vascular reactivity of aortic sections from rabbits fed different diets. A-B Biaxial mechanical properties in terms of Cauchy stress vs. stretch behavior in the circumferential **(A)** and longitudinal **(B)** directions, (n=7)**.** *p<0.05; **p<0.01; ***p<0.001. **C–F Myographical analysis of freshly dissected aortas.** Aortic sections of each rabbit were cut into 4 rings, contracted with modified Krebs-Ringer bicarbonate buffer solution containing high K+ concentration (KPSS) (**C**) and norepinephrine (NE) (**D**) and subsequently relaxed with acetylcholine (Ach) (**E**) and sodium nitroprusside (SNP) (**F**), repeated measurements. In total, 24 rings from 6 rabbits per group were used. In **D-F** mean values for each group are shown. Significant differences are shown in S7.

Supplementary Files

This is a list of supplementary files associated with this preprint. Click to download.

- Supplements16.pdf

- Supplement7.xlsx